Stem Cell Research & Therapy

RESEARCH

Open Access

Therapeutic evaluation of iPSC-derived CD146+ mesenchymal stem cells in ulcerative colitis: biological properties and potential mechanisms

Lv Tian[1,2†], Yiming Wang[2,3†], Lei Shen[4], Mingru Zong[2], Jun Fan[1], Yuxin Lu[3], Xiaochen Cheng[3], Li Du[3*], Lin Zhang[5*] and Fengjun Xiao[3*]

Abstract

Background Mesenchymal stem cells (MSCs) exhibit therapeutic potential for ulcerative colitis (UC) due to their immunomodulatory, homing, and tissue repair capabilities, but clinical efficacy is constrained by heterogeneity. Induced pluripotent stem cell-derived mesenchymal stem cells (iMSCs) exhibit superior stem cell properties compared to traditional MSCs, with CD146+ MSCs exhibiting enhanced biological characteristics. Nevertheless, the biological properties of CD146+iMSCs, as well as their therapeutic potential in UC, remain unclear.

Methods CD146+ subpopulations were isolated from iMSCs and umbilical cord-derived MSCs (UCMSCs) using magnetic beads sorting. The surface markers, proliferation capacity, differentiation potential, and regulatory effects on macrophage polarization were analyzed. Dextran sulfate sodium (DSS) - induced UC mouse models were established and treated with CD146+iMSCs. Body weight, disease activity index (DAI), colon length, and histopathological damage were evaluated. Peripheral immune cells and cytokines were analyzed by flow cytometry and ELISA. Transcriptome sequencing of colon tissues was performed and jointly analyzed with GEO datasets to identify the mechanisms of CD146+iMSCs' therapeutic efficacy in UC through differential gene expression profiling, protein-protein interaction network, functional enrichment analysis, and immune infiltration assessment. The core mechanisms were validated in vitro and vivo.

Results CD146+ iMSCs exhibited similar morphology and macrophage polarization regulatory capacity to CD146+UCMSCs, with superior proliferation and differentiation potential. CD146+ iMSCs significantly ameliorated UC symptoms (weight, DAI), reduced colon damage, decreased IL-6/TNF-α, and restored immune balance. Integrated

[†]Lv Tian and Yiming Wang contributed equally to this work.

*Correspondence:
Li Du
lily5847@163.com
Lin Zhang
linzhang@wmu.edu.cn
Fengjun Xiao
xiaofjun1105@163.com

Full list of author information is available at the end of the article

analysis of colon transcriptome sequencing data and GEO datasets revealed the pivotal role of the IL-17 signaling pathway in the therapeutic effects of CD146+iMSCs. CD146+iMSCs effectively suppressed IL-17 expression both in cell inflammation models and colon tissues, downregulated nine hub genes, and inhibited macrophage polarization via the cGAS-STING axis.

Conclusion CD146+iMSCs exhibited advantages in proliferative and differentiation capabilities. They could ameliorate UC by suppressing IL-17 expression, downregulating HUB genes, and modulating macrophage polarization through the cGAS-STING axis.

Keywords CD146, iPSC-derived mesenchymal stem cells, Ulcerative colitis

Introduction

Ulcerative colitis (UC) is a chronic inflammatory bowel disease (IBD) [1], characterized by chronic inflammation and ulceration of the mucosal layer, typically presenting with alternating periods of flare and remission [2]. It is widely accepted that UC primarily develops in genetically susceptible individuals following exposure to specific environmental triggers [3]. The pathophysiology of UC is highly complex, with factors such as gut microbiota dysbiosis, intestinal epithelial barrier dysfunction, and dysregulated immune responses playing crucial roles in its onset and progression [4, 5]. Over the past two decades, UC has become a global health challenge, with a sharp increase in its occurrence rate in low- and middle-income countries [6, 7]. Current therapeutic strategies for UC include 5-aminosalicylic acid agents, corticosteroids, immunosuppressants, and biologics. However, long-term use of these medications is associated with various adverse effects. Moreover, not all patients respond adequately, and some may develop intolerance [8]. For patients with medically refractory UC, surgical intervention remains a necessary option, although severe complications such as postoperative strictures can significantly impair quality of life [5]. Therefore, there is an urgent need to develop novel treatment strategies.

Mesenchymal stem cells (MSCs) are spindle-shaped cells possessing multilineage differentiation potential and self-renewal capacity [9, 10]. They have been regarded as a profound therapeutic tool widely used in regenerative medicine. Numerous studies have employed MSCs derived from human umbilical cord blood, adipose tissue, bone marrow, and intestinal tissue to treat inflammatory bowel diseases, including UC, demonstrating promising efficacy [11–14]. However, conventional MSCs exhibit high heterogeneity due to variations in tissue sources and isolation techniques, leading to significant differences in surface marker expression, proliferative capacity, and differentiation potential among different subpopulations [15]. Such heterogeneity may influence the immunomodulatory and tissue healing capabilities of MSCs, thereby affecting their therapeutic outcomes in diseases like UC. Hence, developing highly homogeneous MSC subpopulations represents an important future direction for MSC-based therapeutics.

Developing novel stem cell sources has emerged as a promising direction to address the challenge of MSC heterogeneity. Recent advances in stem cell engineering have opened new avenues to address MSC heterogeneity. A novel MSC subtype—induced pluripotent stem cells (iPSCs)-derived MSCs (iMSCs)—has attracted significant attention due to their high homogeneity, enhanced proliferative capacity, and well-preserved self-renewal potential. achieved through the selection of homogenous iPSC clones at an optimal state as the starting population, thereby effectively addressing the challenge of high heterogeneity in the final product. Studies have confirmed that iMSCs are highly similar to adult MSCs in terms of morphology, surface marker expression, stemness-related gene expression, and trilineage differentiation potential [16, 17]. In addition to possessing typical MSC characteristics, iMSCs retain advantages of iPSCs, such as low immunogenicity, reduced senescence, and patient specificity, which lower the risk of immune rejection in recipients during cell therapy [18–23]. These properties enable iMSCs to promote tissue healing significantly [24], modulate immune responses, and attenuate inflammatory reactions [25], making them an up-and-coming cell source in regenerative medicine.

Parallel efforts have focused on isolating functionally distinct subpopulations to address MSC heterogeneity. MSC subpopulations with distinct functional and biological properties have been successfully isolated and purified based on specific surface markers—including Stro-1, SSEA-4, CD271, and CD146 [26–28]. Among these, CD146, an adhesion molecule belonging to the immunoglobulin superfamily, has garnered widespread attention as a functionally relevant surface marker [29–35]. The $CD146^{+}$ MSC subpopulation has demonstrated superior therapeutic efficacy compared with unsorted MSCs across various regenerative medicine models [36–38], suggesting that CD146 may serve as a key marker for defining an MSC subset with enhanced therapeutic potency.

First, the expression of CD146 is directly associated with enhanced homing capacity, which is crucial for

cells to reach sites of intestinal inflammation. Studies have indicated that CD146 serves as a key functional marker promoting the migration and tissue engraftment of MSCs [26–28]. For instance, in a fracture model, CD146+ bone marrow MSCs (BMSCs) exhibited broader tissue distribution and higher chemotactic efficiency [27]; similarly, in an intervertebral disc degeneration model, the CD146+MSCs subpopulation also demonstrated stronger migratory capacity toward injured tissues compared to the CD146- subpopulation [28]. Based on these findings, we hypothesize that CD146+iMSCs are similarly capable of more effectively targeting and accumulating in the intestinal inflammatory and damaged areas of UC, thereby laying the foundation for localized therapeutic effects. Second, CD146+MSCs exhibit superior immunomodulatory functions, particularly their ability to drive macrophage polarization toward the anti-inflammatory M2 phenotype, which aligns closely with UC treatment strategies. In IBD, such as UC, pro-inflammatory M1 macrophages exacerbate inflammation and epithelial barrier damage, whereas anti-inflammatory M2 macrophages are essential for inflammation resolution and mucosal healing [39]. Research has shown that the CD146+MSCs subpopulation holds an advantage in this regard: ex vivo experiments have confirmed their enhanced ability to induce macrophage polarization toward the M2 phenotype, as evidenced by reduced nitric oxide and increased ARG1 expression [40]; more importantly, in vivo studies have demonstrated that CD146+BMSCs pre-stimulated with inflammatory cytokines significantly promote the conversion of M1 to M2 macrophages and secrete higher levels of anti-inflammatory cytokines, thereby more effectively mitigating inflammatory responses [41]. This suggests that CD146+iMSCs may alleviate intestinal inflammation and promote tissue healing in UC by efficiently modulating macrophage balance. Furthermore, beyond macrophage regulation, CD146+MSCs have also demonstrated the ability to modulate adaptive immunity in various disease models (such as premature ovarian insufficiency and sepsis), including reversing the $CD4^+/CD8^+$ T cell ratio imbalance and increasing the proportion of immunosuppressive regulatory T cells [40, 42]. It is particularly noteworthy that their immunosuppressive function can be further amplified under inflammatory microenvironment stimulation. Studies have shown that CD146+BMSCs pre-treated with inflammatory cytokines exhibit a rejuvenated phenotype and highly express key immunomodulatory mediators such as prostaglandin E2 (PGE2) and indoleamine 2,3-dioxygenase [41]. This indicates that CD146+iMSCs can effectively suppress excessive immune responses and robustly respond to inflammatory environments similar to those in UC, thereby enhancing their therapeutic efficacy and providing a strong theoretical possibility for precision medicine in UC treatment.

The aforementioned evidence establishes CD146+MSCs as a highly promising source of therapeutic cells. Previous studies from our laboratory have also confirmed that CD146+ umbilical cord mesenchymal stem cells (UCMSCs) exhibit superior immunomodulatory and pro-regenerative properties. However, whether CD146+ induced pluripotent stem cell-derived MSCs (CD146+iMSCs) possess distinct biological characteristics compared to conventionally sourced MSCs (such as UCMSCs)—particularly within the complex pathological microenvironment of UC—and what their therapeutic potential and mechanisms of action might be, remains unclear. Therefore, this study aims to directly compare the key biological properties of CD146+iMSCs and CD146+UCMSCs, systematically evaluate the therapeutic efficacy of CD146+iMSCs in a UC disease model, and further investigate the underlying molecular mechanisms to provide a novel and potentially superior cell-based therapeutic option for UC.

Methods

Reagents and antibodies

The list of all reagents and antibodies used in this study is recorded in Supplementary file 1 (Table S1).

Isolation of mesenchymal stem cells and cells culture

The human umbilical cords ($n = 3$) were provided by the Beijing Shangdi Hospital. The umbilical cord was washed using normal saline. After cleaning, the vascular structures were removed from the umbilical cord, which was then cut into small pieces and placed in a sterile PBS solution containing 0.05% collagenase and 0.001% hyaluronidase. Subsequently, digestion was performed in a constant temperature shaker at 37 °C and 150 rpm for approximately 2 h. The target cells were obtained through centrifugation and inoculated into the culture flask containing MSCs serum-free medium for culturing. Human iMSCs were purchased from Nuwacell Ltd. (Hefei, China) and were cultured in the ncMission hMSC Medium. HIEC and IEC-6 were cultured in high-glucose DMEM containing 10% FBS and 1% P/S. RAW264.7 was cultured in high-glucose DMEM containing 10% FBS. All cell lines were cultured in a humidified incubator at 37 °C with 5% CO2.

Identification of surface markers

100 μL (1×10^7/mL) of the cell suspension was incubated with specific antibodies for CD73, CD14, CD45, CD34, CD90, CD105, CD106, CD31, and CD11b for 30 min at 4 °C. After washing twice in PBS containing 0.5% FBS, the percentage of cells was detected by flow cytometry.

Sorting of CD146+iMSCs and CD146+UCMSCs

The FcR blocking reagent and CD146 magnetic beads were added to label the cells, and the cells were centrifuged and resuspended. The labeled cells were separated in the magnetic field of the magnetic activated cell sorting (MACS) separator. The cells before and after sorting were incubated with CD146 antibody, incubated at room temperature for 20 min prior to washing in PBS and analyzing by flow cytometry.

Cell proliferation

CD146+iMSCs and CD146+UCMSCs were stained with cell proliferation Dye eFluor 670. The two MSC subpopulations were digested, collected, rinsed with PBS, and resuspended. Then, cells were mixed with Dye670 solution (10 μM) and incubated in the dark at 37 °C for 10 min. Five-fold volumes of complete medium were added and incubated on ice for 5 min to quench staining. Immediately, the cells were washed with complete medium thrice and cultured in MSC complete medium at 37 °C with 5% CO2 at the four-time points (0, 12, 24, and 48 h), respectively. The proliferation index was analyzed with Modfit LTTM.

Cell differentiation

According to the manufacturer's instructions, upon reaching 100% confluence, the complete medium was replaced with MSC adipogenic or osteogenic differentiation medium for 18–21 days or 14–16 days, respectively. After induced differentiation, cells were stained with Oil Red O staining solution for adipogenic differentiation or Alizarin Red solution for osteogenic differentiation. Then, the cells were photographed with an optical microscope.

Construction of a cell inflammation co-culture model

IEC-6 and HIEC were inoculated into six-well plates at a density of 3×10^5 cells per well. Three groups were set up respectively: blank control group (Control group), lipopolysaccharide (LPS) -induced inflammation model group (LPS group), and stem cell co-culture intervention group (CD146+iMSCs group). Then, 1 μg/mL LPS was added to all groups except the control group to induce an inflammation model. In the CD146+iMSCs group, IEC-6 and HIEC were seeded in the lower chambers of the six-well Transwell plate at a density of 3×10^5 cells per well, and MSCs were seeded in the upper chambers at a density of 2×10^5 cells per well. After 36 h, IEC-6 or HIEC were harvested for further experiments.

M1/M2 polarization of RAW264.7

RAW264.7 cells were plated at 1×10^4 cells/ cm^2 in the lower chamber of a six-well Transwell plate in the presence of LPS (1 μg/mL) or Interleukin-4 (IL-4, 20 ng/mL) and two MSC subpopulations were seeded in the upper chambers at a density of 1×10^4 cells/cm^2. Control group, LPS or IL-4 group, LPS or IL-4+CD146+UCMSCs group, and LPS or IL-4+CD146+iMSCs group were established. Each experimental group was cultured in triplicate wells and maintained at 37 °C with 5% CO2. After 48 h, RAW264.7 were harvested and the expression of macrophage-related markers (iNOS, CD206, and Arg-1) were evaluated by flow cytometry and real-time quantitative Polymerase Chain Reaction (RT-PCR).

RNA extraction and RT-PCR

After collecting the cells and the tissues, Trizol and chloroform were added. The mixture was pipetted repeatedly for homogenization, left to stand for 10 min, and then centrifuged at 12,000 rpm for 15 min at 4 °C. After washing the RNA precipitates with 75% ethanol, the supernatant was removed through centrifugation, and the precipitates were air-dried. The RNA concentration was then measured using a spectrophotometer. The reaction system and procedures were established according to the instructions provided in the reverse transcription kit and RT-PCR kit from TransGen Biotech. The relative expression levels of target genes were calculated using the 2-ΔΔCt method. All primer sequences are listed in Supplementary file 1 (Table S2).

RNA sequencing

Two MSC subpopulations (passage 6) and colon samples were frozen in liquid nitrogen and stored at −80 °C. Three samples were randomly selected from each group for RNA sequencing. According to the manufacturer's instructions, total RNA was extracted from the samples using a TRIzol reagent. The integrity and concentration of the RNA were assayed. The cDNA libraries were constructed according to the manufacturer's instructions for the NEBNext Ultra RNA Library Prep Kit for Illumina (E7530; New et al. [NEB], Ipswich, MA, USA) and the NEBNext Multiplex Oligos for Illumina (NEB, E7500). The cDNA libraries were loaded onto an Illumina HiSeq sequencing platform (performed by Applied Protein Technology Company). Adapters and reads in the raw reads of each sample were trimmed to obtain clean reads. Gene expression levels were estimated using Fragments Per Kilobase of exon per Million mapped fragments (FPKM). Differential genes were considered significant when $Padj < 0.05$ and log2 Fold Change $(FC) > 1$. The sequencing data supporting the results are uploaded as supplementary materials (Supplementary file 2 and 3).

Mouse UC model

All animal experiments were approved by the Ethics Committee of the Experimental Animal Center of the Academy of Military Medical Sciences

(IACUC-DWZX-2023-571). All mice were maintained in specific pathogen-free cages at the animal facility and provided with autoclaved food and water. To ensure unbiased group assignment, a total of twenty-four C57BL/6 mice (6–8 weeks old) were randomly allocated into three groups (n = 8 per group) using a random number table method: control group, dextran sulfate sodium (DSS) group and DSS+CD146+iMSCs treatment group. The control group received plain drinking water; DSS group were given 2.5% DSS water for 5 days. On days 3 and 5, 1×10^6 CD146+iMSCs in 0.1 mL PBS were intraperitoneally injected to CD146+iMSCs group, while control and DSS group received PBS vehicle. During the induction and recovery phases of experimental colitis, the mice body weight, faecal characteristics, and faecal occult blood test were recorded daily. The disease activity index (DAI) [43] was calculated daily according to the previous protocol. On day 10 of the modeling process, the mice were sacrificed via spinal dislocation to facilitate subsequent sampling and testing (Fig. 4B). The work has been reported in line with the ARRIVE guidelines 2.0.

In vivo small animals imaging

C57BL/6 mice (6–8 weeks old) were divided into two groups using a random number table method: tail vein injection groups and intraperitoneal injection groups (n = 6 per group), with each group further subdivided into control group and DSS group (n = 3 per group). CD146+iMSCs were co-incubated with 10 μM DIR solution in a 37 ℃ incubator for 30 min. Then 1×10^6 DIR-labeled CD146+iMSCs were injected into mice in the DSS group by intraperitoneal injection or tail vein injection, respectively. Mice were anesthetized with 3–5% isoflurane (in 100% oxygen at 0.4–0.6 L/min flow rate) using a precision vaporizer. Induction was performed in a sealed chamber for 2 min until loss of righting reflex was observed. Afterward, the abdominal hair of the mice was removed, and fluorescence images of the cells were captured using a small animal in vivo imaging system on days 1, 3, 7, 14, 21, and 28 post-injection. At the end of imaging on day 28, the overall fluorescence intensity scale was adjusted for normalization analysis.

Animal anesthesia

Anesthesia procedure for in vivo small animals imaging: Isoflurane was introduced into the vaporizer, and the anesthesia machine along with the oxygen supply system was activated. The oxygen flow rate was adjusted to 0.4–0.6 L/min, with the initial isoflurane concentration set at 3%–5%. The mouse was then gently placed into the induction chamber and maintained under sealed conditions for 2 min. Anesthesia protocol for mouse sample collection: 1% sodium pentobarbital solution was prepared in physiological saline. Anesthesia was administered via intraperitoneal injection at a dosage of 50 mg/kg body weight.

Hematoxylin and eosin staining (H&E staining)

Colon tissues were collected at the end of the study period and immediately fixed with 4% paraformaldehyde. The tissue samples were embedded in paraffin and stained with hematoxylin and eosin. The specimens were observed and photographed under an inverted microscope. A total of 5 fields per group was selected randomly and histological examinations were performed in a blinded manner. The severity of symptoms was calculated by scoring the extent of bowel wall thickening (grades 0–3: 0, none; 1, mucosa; 2, mucosa and submucosa; 3, transmural), damage to the crypt (grades 0–3: 0, none; 1, loss of goblet cells; 2, only surface epithelium intact; 3, loss of entire crypt and epithelium), and infiltration of inflammatory cells (grades 0–2: 0, none; 1, mild to moderate; 2, severe).

Peripheral blood test and immune phenotyping

Blood samples were collected from the orbital vein. 20–30 μL of EDTA anticoagulated blood was mixed evenly and analyzed using an automated hematology analyzer. 50 μL of EDTA-anticoagulated blood were incubated with CD3, CD4, CD8, CD11b, and B220 flow antibodies in the dark at 4 °C for 30 min. Subsequently, 1× red blood cell lysis buffer was added, and lysis was performed at room temperature for 10–15 min. After lysis was complete, flow cytometry was used for detection, and the data were analyzed using FlowJo software.

Enzyme-linked immunosorbent assay (ELISA)

Blood samples were collected from the orbital vein and centrifuged at 3000 rpm for 15 min to obtain serum. According to the manufacturer's instructions, the levels of IL-6 and tumor necrosis factor-alpha (TNF-α) in the serum were measured using an ELISA kit.

Data source

Four ulcerative colitis datasets were downloaded from the GEO database (https://www.ncbi.nlm.nih.gov/geo/), and GEOquery (version 2.54.1) was used.

Differentially expressed genes (DEGs) screening

The data in the four datasets were obtained by removing probes corresponding to multiple molecules. There may be cases where one molecule corresponds to multiple probes, or one probe corresponds to multiple molecules. For multiple probes corresponding to the same molecule, only the probe with the largest signal value was retained. The data was then normalized once more using the normalize Between Arrays function of the limma package (version 3.42.2). The clustering patterns among sample

groups were examined using Principal Component Analysis (PCA) plot. Differential analysis between two groups was performed using the limma package, and the results were visualized with volcano plots (with thresholds set at $|\log2(FC)| > 1$ and $p.adj < 0.05$). Additionally, significantly expressed molecules are visualized using heatmaps. All statistical analyses and visualizations were performed using R (version 3.6.3).

Protein-protein interaction network construction and key HUB gene identification

Four GEO datasets (GSE87466, GSE47908, GSE36807, and GSE9452) were analyzed for the differential expressed genes and the results were visualized using ggplot2 (version 3.3.6) and Venn Diagram (version 1.7.3). The common DEGs were used to construct a protein-protein interaction (PPI) network based on Search Tool for the Retrieval of Interacting Genes (STRING) database, and significant modules were analyzed and their key genes were screened by using Cytoscape software. Subsequently, the cytohubba algorithm was employed to identify HUB genes, followed by the creation of a HUB network diagram.

DEGs enrichment analysis

Common DEGs (human source) were annotated using the org.Hs.eg.db (version 3.10.0) for ID conversion. Subsequently, functional enrichment analysis, including Gene Ontology (GO) terms and Kyoto Encyclopedia of Genes and Genomes (KEGG) pathways, was performed on these shared DEGs with the clusterProfiler package (v3.14.3).

Immune infiltration analysis

We used the CIBERSORTx website (https://CIBERSORTx.stanford.edu/) to estimate the correlation between HUB genes and immune cells in the samples from the GSE87466, GSE47908, GSE36807, and GSE9452 datasets. The results were visualized using GraphPad Prism 8.

Western blot (WB)

RAW264.7 cells and colon tissues were lysed using RIPA lysis buffer. SDS loading buffer was added to the samples, which were then incubated at 100 °C for 10 min. The sample proteins were separated by 4–20% SDS-PAGE gel electrophoresis and transferred to a 0.45 μm polyvinylidene fluoride membrane. The proteins were blocked with Tris-buffered saline containing 5% skim milk powder. Subsequently, the samples were co-incubated with antibodies (β-Actin, IL-17, cGAS, and STING) overnight at 4 °C. The membrane was then co-incubated with horseradish peroxidase (HRP)—conjugated Goat Anti-Rabbit IgG (H+L). The protein bands were treated with an enhanced chemiluminescence (ECL) kit for visualization and analyzed by Image J software.

Statistical analysis

Data are expressed as mean ± standard error (M ± SEM). All statistical analyses were performed with GraphPad Prism software. All results were from three independent experiments. Differences among three or more groups were analyzed by one-way ANOVA followed by Tukey's multiple-comparison test. Differences between two groups were evaluated by unpaired two-tailed t-tests. Post hoc tests were performed using the Tukey test. All experiments were repeated independently three times. $P < 0.05$ was considered statistically significant.

Results

Acquisition and identification of iMSCs and UCMSCs

Cryopreserved iMSCs were thawed and expanded to the 4th passage (P4), exhibiting a typical fibroblast-like morphology (Fig. 1A). UCMSCs were successfully obtained using a standard isolation protocol and cultured to P4, showing similar morphological characteristics (Fig. 1B). Flow cytometry analysis revealed that both cell types expressed typical MSCs markers (CD73, CD90, and CD105; positivity rate > 95%), while were negative for hematopoietic/endothelial lineage markers (CD11b, CD14, CD31, CD34, CD45, and CD106) (Fig. 1C, D). These findings confirm that both iMSCs and UCMSCs meet the minimal criteria for MSCs established by the International Society for Cellular Therapy (ISCT).

Biological characteristics of CD146+iMSCs and CD146+UCMSCs

We obtained CD146+iMSCs and CD146+UCMSCs using CD146 immunomagnetic bead separation (Fig. 2A). Flow cytometry analysis revealed that the proportions of CD146+ cells in iMSCs and UCMSCs before separation were 15.5% and 25.7%, respectively, and the purity after separation was over 97% for both cell types (Fig. 2B). The magnetic bead separation process did not affect cell morphology, and both stem cell subpopulations maintained typical spindle-shaped adherent growth characteristics (Fig. 2C). As shown in Fig. 2D, differentiation experiments demonstrated that both CD146+iMSCs and CD146+UCMSCs possess adipogenic and osteogenic differentiation potential. However, CD146+iMSCs exhibited stronger differentiation capacity, as evidenced by increased calcified deposits after osteogenic induction and a higher number of lipid droplets with a larger stained area after adipogenic induction. Quantitative histomorphometry further revealed statistically significant differences in both Alizarin Red-positive area (osteogenesis) and Oil Red O-positive area (adipogenesis) between CD146+iMSCs and CD146+UCMSCs (Fig. 2E). For Dye

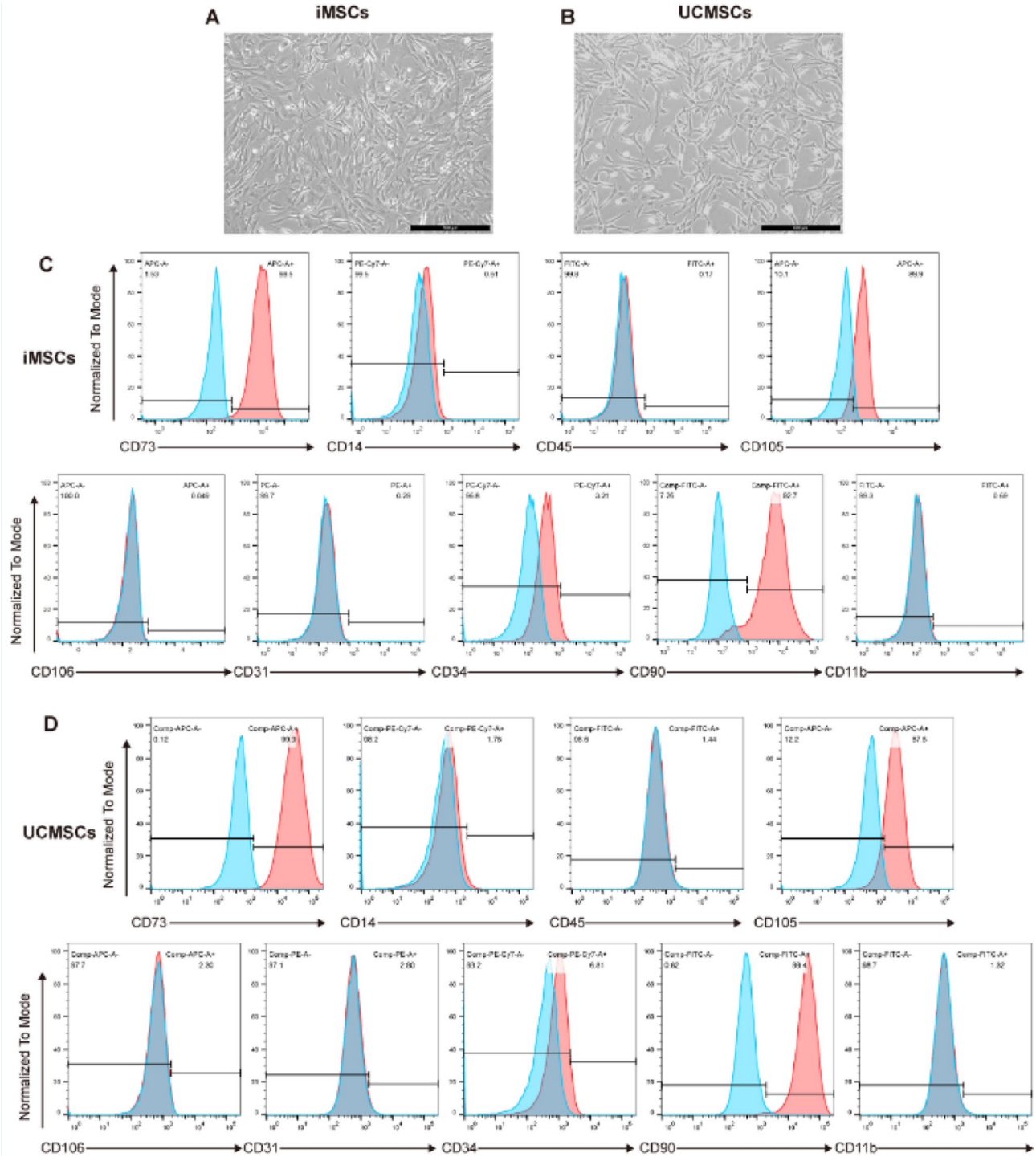

Fig. 1 Acquisition and identification of iMSCs and UCMSCs. **A** Morphology of iMSCs (10×, scale bar: 500 μm). **B** Morphology of UCMSCs (10×, scale bar: 500 μm). **C** Flow cytometry analysis of surface markers of iMSCs ($n = 3$). **D** Flow cytometry analysis of surface markers of UCMSCs ($n = 3$)

eFluor 670 proliferation assay (Fig. 2F), CD146+iMSCs exhibited significantly higher proliferation ability than that of CD146+UCMSCs (Fig. 2G). Flow cytometry results indicated that compared to the LPS group or IL-4 group, treatment with both stem cell subpopulations reduced the proportion of M1—macrophages (iNOS+) and increased the proportion of M2—macrophages (CD206+) (Fig. 2H). In addition, qPCR results further confirmed that compared to the LPS group or IL-4 group, both stem cell subgroups significantly inhibited the expression of the M1 marker iNOS (Fig. 2I) and promoted the expression of the M2 marker Arg-1

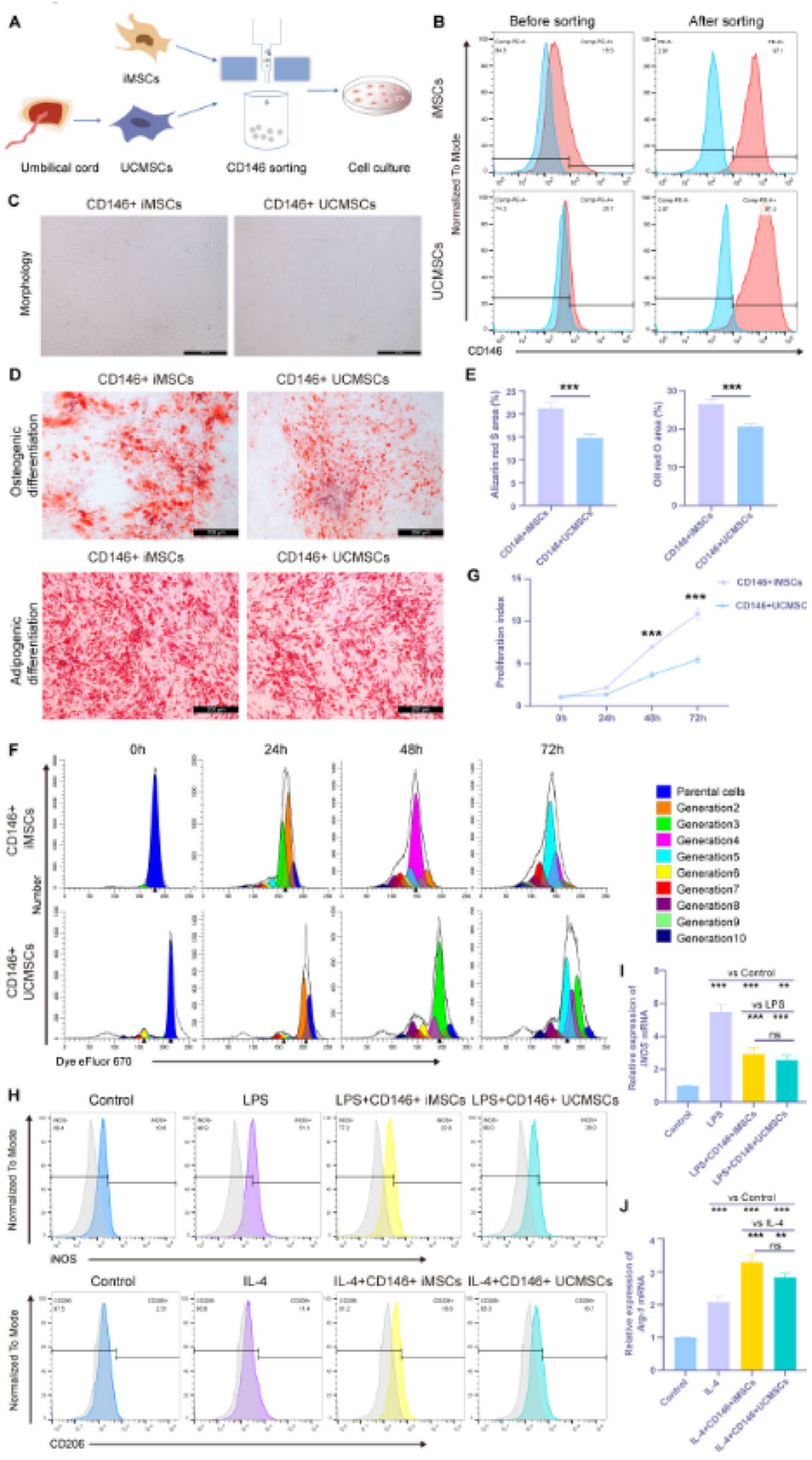

Fig. 2 (See legend on next page.)

(See figure on previous page.)

Fig. 2 Biological characteristics of CD146+iMSCs and CD146+UCMSCs. **A** Schematic diagram of magnetic bead sorting. **B** Flow cytometry analysis of the expression of CD146 in iMSCs and UCMSCs before and after magnetic bead sorting ($n=3$). **C** Cell morphology after magnetic bead sorting (10×, scale bar: 500 μm). **D** Alizarin Red staining for osteogenic differentiation and Oil Ted O staining for adipogenic differentiation (10×, scale bar: 200 μm). **E** Quantitative analysis of osteogenic differentiation and adipogenic differentiation ($n=3$). **F** CD146+iMSCs and CD146+UCMSCs were incubated with Dye eFluor 670, and cell proliferation was evaluated by flow cytometry at 0 h, 12 h, 24 h, and 48 h ($n=3$). **G** The cell proliferation index of CD146+iMSCs and CD146+UCMSCs ($n=3$). **H** Flow cytometry analysis of macrophage polarization ($n=3$). **I** RT-PCR results of the macrophage polarization marker iNOS (M1) ($n=4$). **J** RT-PCR results of the macrophage polarization marker Arg-1 (M2) ($n=4$). Performed in duplicate from three independent experiments. Data are presented as mean ± SEM. For all graphs, $^{**}p<0.01$, $^{***}p<0.001$

(Fig. 2J). However, there was no statistically significant difference in regulatory ability between the two stem cell subpopulations.

Transcriptome sequencing of CD146+iMSCs and CD146+UCMSCs

After comparing the biological characteristics of CD146+iMSCs and CD146+UCMSCs, we further conducted RNA sequencing analysis on these two stem cell subpopulations of passage 6 to deeply explore their functional differences. The sequencing results revealed 2720 differentially expressed genes between the CD146+iMSCs group and the CD146+UCMSCs group, including 1596 upregulated genes and 1124 downregulated genes (Fig. 3A). Figures 3B and C present the visual volcano plot and hierarchical clustering diagram of these DEGs between the CD146+iMSCs group and the CD146+UCMSCs group, respectively. Among the significantly upregulated pathways, CD146+iMSCs exhibited strong activation of the neuroactive ligand–receptor interaction pathway and the calcium signaling pathway (Fig. 3D). Multiple genes encoding neurotransmitter receptors (e.g., HTR2A, ADRA1B) and ion channels (e.g., CACNA1C, CACNB1) were upregulated, suggesting that CD146+iMSCs may possess enhanced basal signal perception and transmembrane signal transduction activity. Furthermore, in CD146+iMSCs, the expression of core ligand genes (TGFB2, TGFB3) and regulatory factors (SMAD6) of the TGF-β signaling pathway was upregulated. Key molecules in the intestinal immune network for IgA production, such as the B-cell activation factor CD40 and the lymphocyte chemoattractant CXCL12, were also consistently upregulated. These transcriptional changes indicate potential roles in immunomodulation and mucosal barrier repair. On the other hand, among the significantly downregulated pathways, the TNF signaling pathway was broadly suppressed in CD146+iMSCs (Fig. 3E). Upstream signaling molecules (MAP3K8, MAP3K5), pro-inflammatory cytokines (IL1B, IL6), and downstream effectors (MMP3, PTGS2) within this pathway were all markedly downregulated. These results suggest that CD146+iMSCs may exert anti-inflammatory effects by suppressing the TNF signaling pathway. In terms of cellular components (CC) (Fig. 3F), differentially expressed genes were significantly enriched in the extracellular matrix and integral components of the plasma membrane, indicating that CD146+iMSCs may have enhanced cell surface interaction capabilities and secretory functions, which are crucial for repairing the damaged intestinal mucosal physical barrier in UC. Differentially expressed genes were enriched explicitly at the molecular function (MF) level in terms such as signaling receptor regulator activity and receptor ligand activity (Fig. 3F). Within these pathways, chemokine (e.g., CXCL12) and growth factors (e.g., VEGF, FGF) were significantly upregulated, providing a molecular basis for their immunomodulatory functions and paracrine signaling activity.

Evaluation of the therapeutic efficacy of intraperitoneal injection of CD146+iMSCs in DSS-induced UC

The therapeutic efficacy of MSCs is influenced by different administration routes. To determine the optimal route, we first compared the in vivo biodistribution of CD146+iMSCs administered via intraperitoneal injection and tail vein injection using a small animal in vivo imaging system. We found that the fluorescence signals in the intraperitoneal injection group were mainly enriched in the abdominal region of the mice and persisted for a longer duration (Fig. 4A). Therefore, we selected intraperitoneal injection for subsequent treatment experiments. As shown in the schematic diagram (Fig. 4B), we established a mouse UC model and administered CD146+iMSCs via intraperitoneal injection to systematically evaluate their efficacy in treating UC. The body weight of mice in the DSS group decreased significantly during modeling, whereas the weight loss in the CD146+iMSCs group was significantly attenuated compared to the DSS group (Fig. 4C). Additionally, the disease activity index score was significantly lower in the CD146+iMSCs group compared to the DSS group (Fig. 4D). We further examined colon length and morphology. Compared to the control group, the colon in the DSS group was significantly shortened and exhibited congestion and edema, while the colon length in the CD146+iMSCs group was less shortened, and the redness and swelling were improved (Fig. 4E, F). H&E staining revealed abnormal colonic crypt structure and abnormal inflammatory cell infiltration in the DSS group, whereas the crypt structure and epithelial cell structure were better preserved in the CD146+iMSCs group, and the histopathological activity index was reduced compared to the DSS group (Fig. 4G,

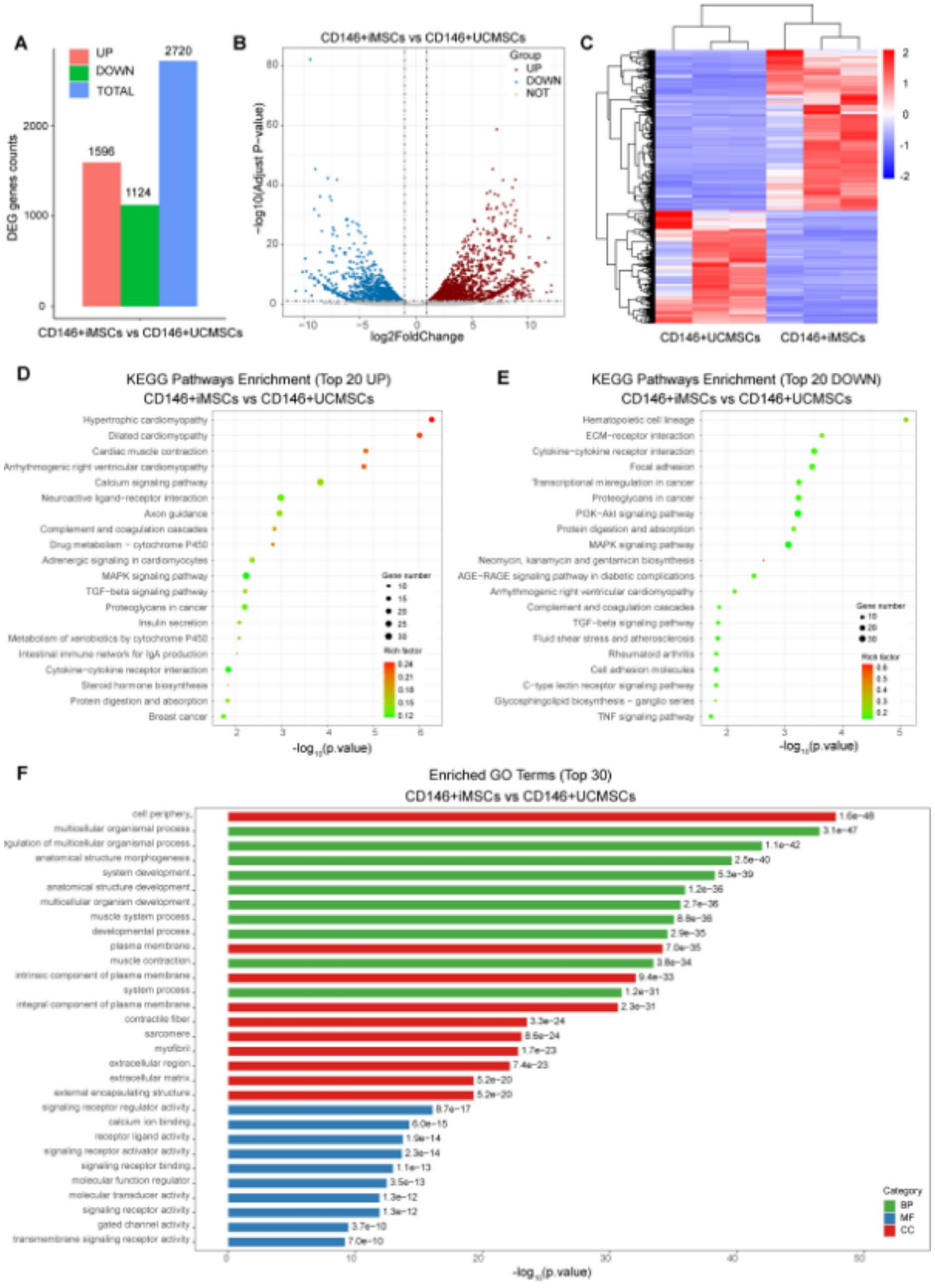

Fig. 3 (See legend on next page.)

(See figure on previous page.)

Fig. 3 Transcriptome sequencing of CD146+iMSCs and CD146+UCMSCs. **A** Histogram of differentially expressed genes (DEGs) ($n = 3$, CD146+iMSCs vs. CD146+UCMSCs). **B** Volcano plot of DEGs (CD146+iMSCs vs. CD146+UCMSCs). **C** Hierarchical clustering diagram of DEGs (CD146+iMSCs vs. CD146+UCMSCs). **D** Bubble plot of KEGG pathway enrichment analysis (TOP20 UP, CD146+iMSCs vs. CD146+UCMSCs). **E** Bubble plot of KEGG pathway enrichment analysis (TOP20 DOWN, CD146+iMSCs vs. CD146+UCMSCs). **F** Multi-panel bar plots of GO enrichment terms (TOP30, CD146+iMSCs vs. CD146+UCMSCs)

H). Immunohistochemistry results showed that compared with the DSS group, the Zonula Occludens-1 (ZO-1) protein expression pattern in the CD146+iMSCs group was similar to that in the control group, maintaining an intact epithelial barrier structure (Fig. 4I). These findings strongly demonstrate that CD146+iMSCs can effectively alleviate DSS-induced ulcerative colitis in mice.

CD146+iMSCs restore peripheral immune homeostasis and suppress Proinflammatory cytokines in UC

To elucidate the immunomodulatory profile of CD146+iMSCs in alleviating UC, we documented coordinated changes in inflammatory parameters. Peripheral blood test results showed typical inflammatory blood alterations in the DSS group, characterized by a decrease in white blood cells (WBC) and abnormal elevations in red blood cells (RBC), platelets (PLT), and hemoglobin (HGB). Treatment with CD146+iMSCs reversed these abnormal indicators, significantly restoring peripheral blood counts to levels comparable to those of normal mice in the control group (Fig. 5A). Flow cytometry analysis of peripheral immune cell profiling further untangled that CD146+iMSCs effectively modulate the balance of peripheral immune cells. As shown in Fig. 5B, CD146+iMSCs normalized the levels of CD3+ T cells, myeloid CD11b+ cells, and the CD4/CD8 ratio in peripheral blood from the UC model. Examination of inflammatory cytokines revealed that DSS induction significantly increased the levels of proinflammatory cytokines IL-6 and TNF-α in mouse serum, as well as the expression of IL-6, TNF-α, and IL-1β in colonic tissue. However, treatment with CD146+iMSCs significantly downregulated the levels of these proinflammatory cytokines (Fig. 5C, D). Thus, these findings validated that CD146+iMSCs suppress inflammation responses by affecting cytokines and lymphocytes. These coordinated changes warrant further investigation and provide a foundation for the development of CD146+iMSCs-based treatment plans for UC.

Integrated bioinformatics and transcriptomics reveal IL-17 signaling pathway in ulcerative colitis pathogenesis

This study conducted a comprehensive analysis of four ulcerative colitis datasets (GSE9452, GSE36807, GSE87466, and GSE47908) from the GEO database. Additionally, transcriptome sequencing was performed on colon tissue from control and DSS-treated mice. The combined results were used to explore the pathophysiology of ulcerative colitis.

As shown in Fig. 6A, the PCA results demonstrate a clear spatial separation between the healthy control group and the UC group samples across the four datasets. The independent clustering of the two groups in the principal component space indicates significant differences between them, suggesting reliable data. The volcano plots display 2400, 1279, 3117, and 1280 DEGs identified in the four datasets, respectively (Fig. 6B). The Venn analysis revealed 132 common DEGs shared among the four datasets (Fig. 6C), which were then input into the String database for interaction analysis and to construct a protein-protein interaction network (Fig. 6D). Using the cytohubba algorithm, nine key HUB genes were identified: ISG20, GBP1, PSMB8, ISG15, IFITM1, GBP2, GBP5, CXCL10, and OAS2 (Fig. 6E). The KEGG enrichment analysis of the 132 DEGs suggested that the occurrence of UC was associated with NOD-like receptor signaling pathway, complement and coagulation cascades, and IL-17 signaling pathway (Fig. 6F). The GO analysis results (Fig. 6G, H) indicated that DEGs were involved in cytokine-mediated signaling pathway, positive regulation of inflammatory response, granulocyte chemotaxis, and response to interferon-gamma. They were also related to cellular components such as secretory granule lumen, cytoplasmic vesicle lumen, and collagen-containing extracellular matrix.

The sequencing results of mice colon showed that 2177 DEGs were found in the DSS group compared to the Control group (Fig. 6I). Figure 6J visualized the TOP10 results of GO analysis, revealed that these DEGs were associated with biological processes such as response to external stimulus, regulation of multicellular organismal processes, and cell migration. Additionally, these genes were involved in cellular components including the cell periphery, plasma membrane, and extracellular region. Furthermore, they participated in molecular functions like signaling receptor binding, calcium ion binding, receptor ligand activity, and extracellular matrix binding. The TOP20 results of KEGG enrichment analysis indicated that these DEGs were enriched in signaling pathways such as cytokine-cytokine receptor interaction, IL-17 signaling pathway, and complement and coagulation cascades (Fig. 6K).

The enrichment of the IL-17 signaling pathway in both clinical samples and mouse tissue samples suggests that IL-17-related inflammatory pathways may play a critical

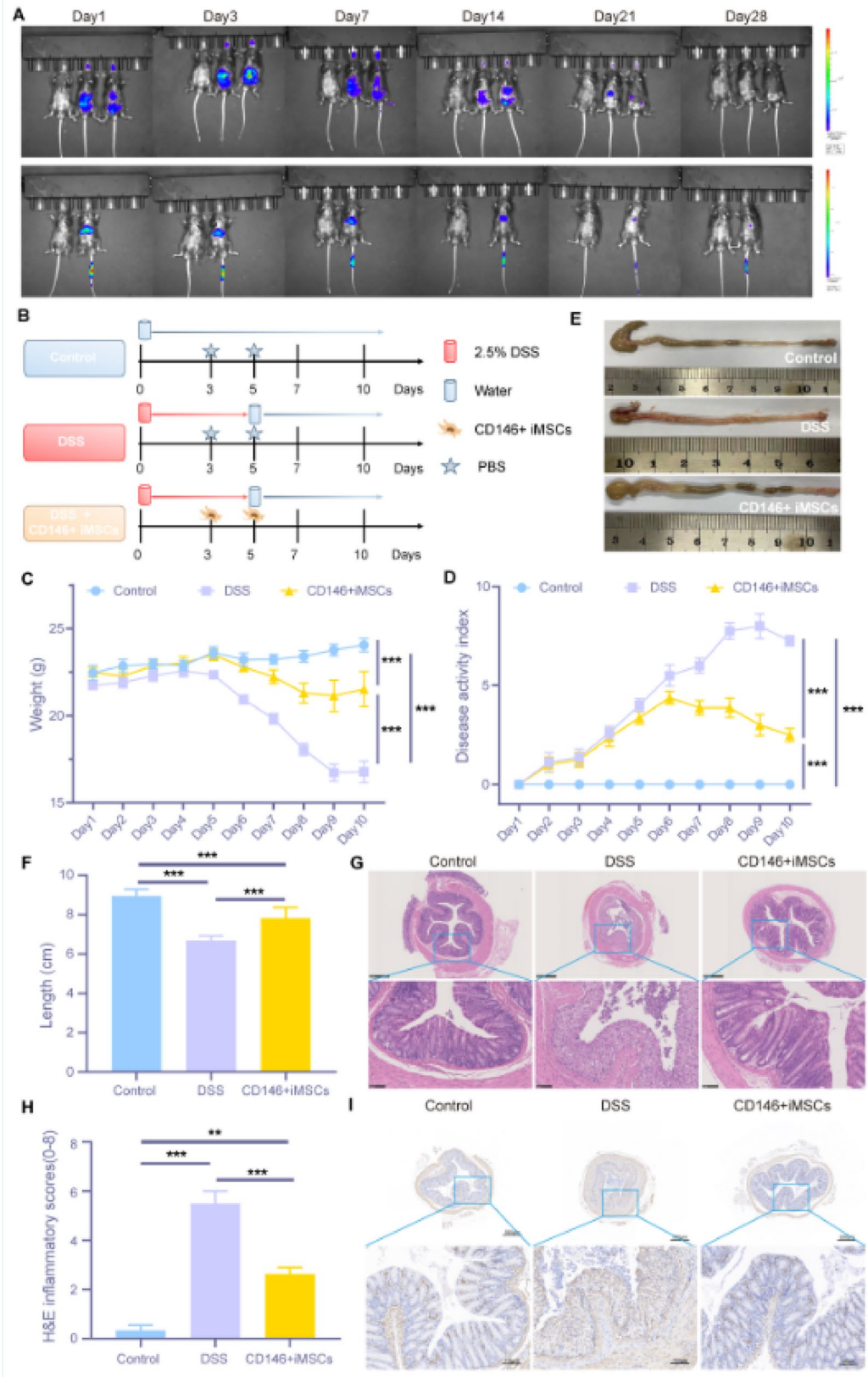

Fig. 4 (See legend on next page.)

(See figure on previous page.)

Fig. 4 CD146+iMSCs could alleviate DSS-induced ulcerative colitis in mice. **A** The in vivo biodistribution of CD146+iMSCs administered via intraperitoneal injection (upper, $n=3$) and tail vein injection (lower, $n=2$). **B** Schematic diagram of the construction of the mouse UC model: control group ($n=6$), DSS group ($n=8$), and DSS+CD146+iMSCs group ($n=8$). **C** Daily body weight in three groups. **D** Disease activity index in each group. **E** Representative photographs of colons in each group. **F** Comparison of colon lengths among three groups. **G** Representative Hematoxylin and eosin staining images of colon from three groups. **H** Histopathological Scores. **I** Representative immunohistochemical image of ZO-1 in colonic tissues. $^{**}p<0.01$, $^{***}p<0.001$

role in the occurrence and development of ulcerative colitis.

CD146+iMSCs attenuate colitis via IL-17 signaling Inhibition and hub gene network modulation

The WB analysis of the colon tissue revealed a significant upregulation of IL-17 expression in the DSS group, which was notably downregulated following treatment with CD146+iMSCs (Fig. 7A, B). In the LPS-induced inflammatory cell co-culture model, CD146+iMSCs significantly decreased the expression of nine HUB genes in both HIEC and IEC-6 compared to the LPS group (Fig. 7C, D).

CD146+iMSCs regulate macrophage polarization through cGAS-STING axis

Based on the established anti-inflammatory effects of CD146+iMSCs, we further explored their regulatory mechanisms on the immune microenvironment. Immune infiltration analysis revealed that macrophage polarization played a significant role in the pathogenesis of UC: the proportion of M0 macrophages was significantly reduced in the UC group, while the infiltration of proinflammatory M1 subtype macrophages was markedly increased (Fig. 8A). Results on the biological characteristics of CD146+iMSCs indicated their ability to inhibit the polarization of M0 macrophages towards M1 macrophages and promote the conversion of M0 macrophages to M2 macrophages (Fig. 2H–J). To investigate whether CD146+iMSCs improve UC by modulating macrophage polarization, we conducted in vitro and in vivo experiments for validation. As shown in the immunofluorescence results of colonic tissue in Fig. 8B, the DSS group exhibited increased infiltration of M1 macrophages compared to the control group, which was significantly reduced following CD146+iMSCs treatment. WB analysis further demonstrated that CD146+iMSCs could downregulate the expression of proteins in the cGAS-STING pathway in LPS-induced macrophages (Fig. 8C, D). These findings suggest that CD146+iMSCs may inhibit the transition of macrophages from the M0 to the M1 phenotype, at least in part through suppression of the cGAS-STING signaling pathway, thereby improving colonic inflammation.

Discussion

Mesenchymal stem cells are multipotent cells characterized by their multi-directional differentiation potential, self-renewal capacity, secretory properties of trophic factors, and homing ability to inflammation or tissue injury sites. Owing to these properties, MSCs have emerged as promising candidates for cell-based therapy in various diseases, including inflammatory bowel disease. However, the biological characteristics and therapeutic efficacy of MSCs vary considerably depending on their tissue origin and cellular subpopulations. This study evaluated the similarities and differences in the biological properties of CD146+iMSCs and CD146+UCMSCs. Further, it demonstrated that intraperitoneal injection of CD146+iMSCs significantly alleviated symptoms in a murine model of DSS-induced UC. Mechanistic studies suggested that the beneficial effects of CD146+iMSCs may be associated with modulation of the IL-17 signaling pathway and macrophage polarization.

CD146 is a mesenchymal marker of MSCs [26–28, 35]. Compared with CD146- cells, CD146+MSCs exhibit enhanced multilineage differentiation potential and immunomodulatory capacity ex vivo [36–38, 41], suggesting the value of this marker in identifying MSC subpopulations with therapeutic potential. However, due to variations in tissue origin and microenvironment, whether CD146+MSCs exhibit consistent functional properties remains to be elucidated. This study focused on CD146+iMSCs and compared their biological characteristics with those of $CD146^{+}$ UCMSCs. The results showed that both cell types shared similar morphology, met the surface marker criteria for MSCs, and possessed comparable ability to regulate macrophage polarization. CD146+iMSCs demonstrated a superior proliferation rate and multilineage differentiation potential. This finding is consistent with previous reports indicating that iMSCs exhibit greater expansion capacity and long-term culture stability than conventionally sourced MSCs, and can maintain MSCs characteristics even after multiple passages ex vivo [44, 45]. The underlying mechanism may involve the erasure of senescence-associated methylation marks and the retention of partial epigenetic memory during reprogramming, which helps maintain stable gene expression profiles and consistent surface antigen presentation during long-term expansion [21, 46, 47]. Moreover, sustained high expression of endogenous pluripotency markers such as Oct4 may also contribute to the maintenance of stemness in iMSCs [46].

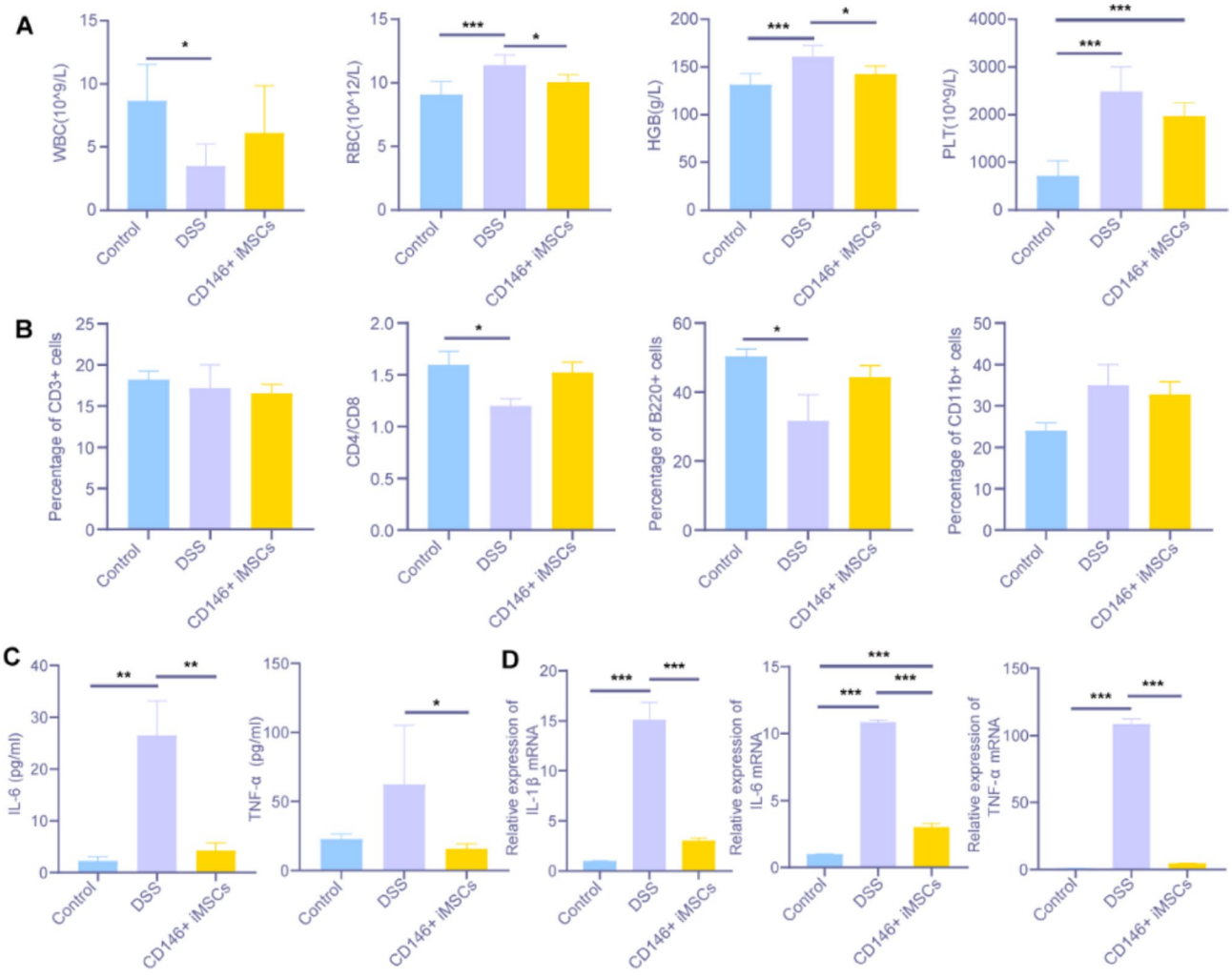

Fig. 5 CD146+iMSCs Could Inhibit Inflammatory Responses in UC. **A** Peripheral blood test in control group ($n=6$), DSS group ($n=7$) and CD146+iMSCs group ($n=7$). **B** Flow cytometry analysis of the proportion of immune cells in peripheral blood ($n=6$ in control group, $n=6$ in DSS group and $n=7$ in CD146+iMSCs group). **C** ELISA analysis of IL-6 and TNF-α expression in peripheral blood among three groups ($n=5$ in each group). **D** RT-PCR analysis of mRNA levels of IL-1β, IL-6, and TNF-α in colonic tissue among three groups ($n=4$ in each group). *$p<0.05$, **$p<0.01$, ***$p<0.001$

In this study, a DSS-induced UC model was employed, which recapitulates the pathological features of human IBD by disrupting the intestinal epithelial barrier and activating the innate immune response. This model is widely used for evaluating the therapeutic efficacy of MSCs [48]. Following DSS induction, mice exhibited shortened colon length, and histological examination revealed structural damage to the colonic mucosa, loss of crypts, and downregulated expression of the tight junction protein ZO-1, indicating severe impairment of the intestinal barrier function. Concurrently, significantly elevated levels of inflammatory cytokines were observed in serum and local colonic tissues, further confirming aberrant immune response activation. The aforementioned pathological changes were markedly alleviated after intraperitoneal administration of CD146+iMSCs. The mucosal structure and intestinal barrier integrity were restored, and inflammatory responses in the circulation and damaged colonic sites were significantly suppressed. These findings are consistent with previous studies indicating that MSCs can ameliorate experimental colitis by preserving the epithelial barrier structure and modulating immune responses [11–14]. Notably, the superior therapeutic effects observed in this study may be attributed to the distinct transcriptomic signatures of CD146+iMSCs. As mentioned earlier, factors associated with signaling receptor regulator activity (such as CXCL12 and FGF) were significantly upregulated in CD146+iMSCs, suggesting that CD146+iMSCs may enhance barrier repair through potentiated paracrine functions. Moreover, widespread suppression of the TNF signaling pathway and upregulation of the TGF-β signaling pathway provide a molecular basis for their robust anti-inflammatory and pro-repair phenotype.

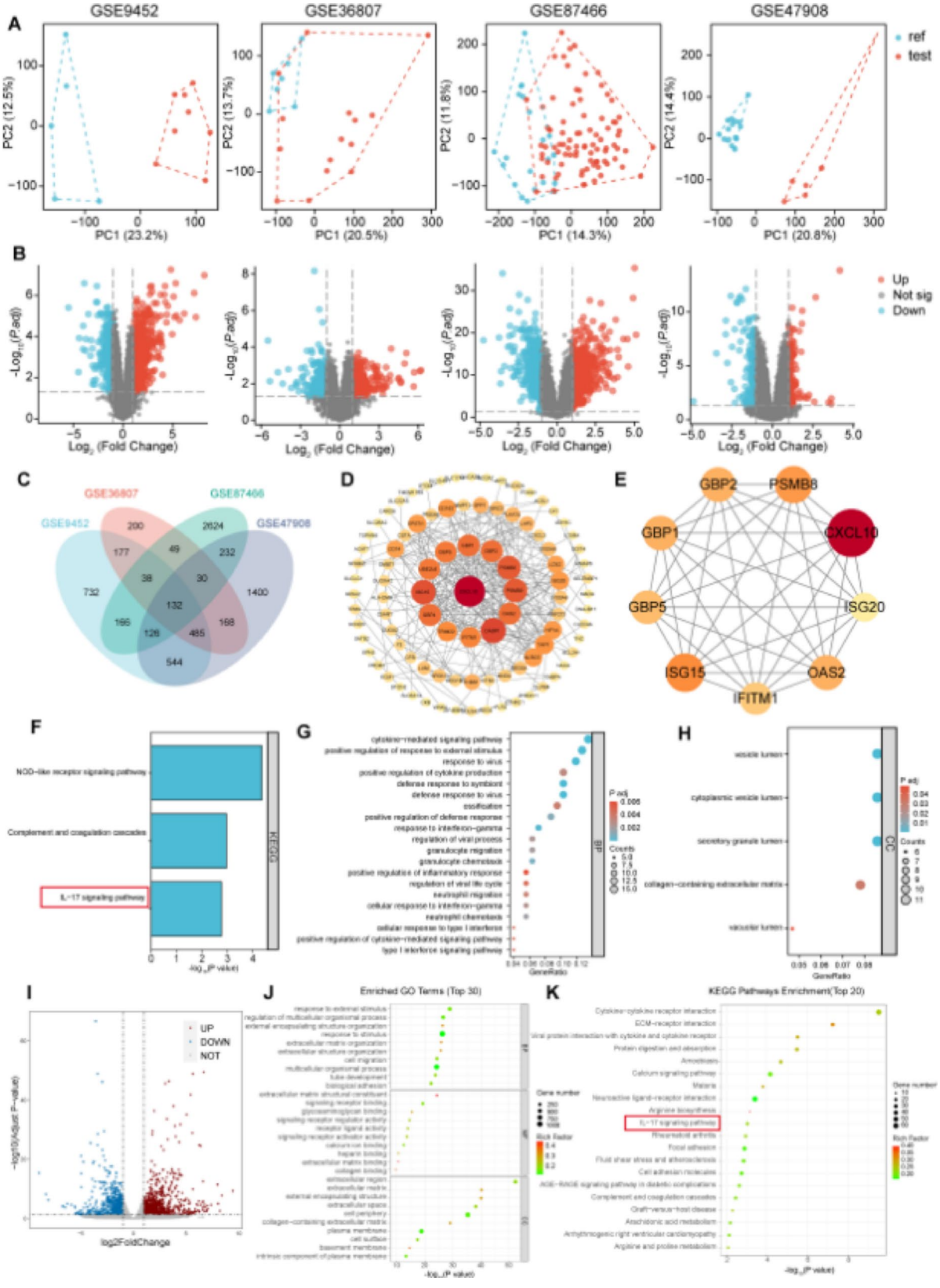

Fig. 6 (See legend on next page.)

(See figure on previous page.)

Fig. 6 Transcriptome analysis of ulcerative colitis datasets and colon tissues. **A** PCA plots of UC dataset GSE9452, GSE36807, GSE87466, and GSE47908. **B** Volcano plots of DEGs in four UC datasets. **C** Venn diagram of DEGs in four UC datasets. **D** Protein-Protein interaction (PPI) network of 132 shared DEGs. **E** PPI network diagram of nine HUB genes. **F** Bar chart of KEGG pathway analysis for 132 shared DEGs. **G** Bubble plot of the GO analysis for biological process of 132 shared DEGs. **H** Bubble plot illustrating the GO analysis for cellular component of 132 shared DEGs. **I** Volcano plot showing DEGs in the colon tissues of UC group and control group. **J** Bubble plots of GO enrichment analysis for DEGs from **I**. **K** Bubble plot of KEGG pathway enrichment analysis for DEGs from **I**

Nevertheless, the precise mechanisms of action of CD146+iMSCs—particularly the relative contributions of their direct effects on intestinal epithelial cells versus their immunomodulatory effects—warrant further investigation.

To elucidate the underlying mechanisms by which CD146+iMSCs ameliorate UC, this study integrated four UC datasets from the GEO database, identifying 132 common differentially expressed genes. KEGG enrichment analysis revealed that these genes were enriched in multiple inflammation-related pathways, with the IL-17 signaling pathway significantly enriched. Notably, enrichment of the IL-17 signaling pathway was also observed in colon transcriptome data from our DSS-induced UC mouse model. To validate the role of the IL-17 pathway, the expression of its key factors was examined in the UC mouse model. It was found that CD146+iMSCs treatment significantly reduced the protein expression level of IL-17 in colon tissues, suggesting that this pathway may mediate the immunomodulatory effects of CD146+iMSCs. IL-17 is a pro-inflammatory cytokine primarily secreted by immune cells such as Th17 cells and γδ T cells. It promotes inflammatory responses by activating the NF-κB and MAPK pathways and can synergize with factors such as TNF-α to amplify inflammatory signals [49–53]. Immune infiltration analysis of UC patient data in this study indicated increased infiltration of M1 macrophages, $CD8^+$ T cells, and γδ T cells, which was closely associated with elevated IL-17 levels. Previous studies have reported that MSCs can reduce IL-17 levels by inhibiting Th17 cell differentiation and promoting regulatory T cell priming [54–56]. Consistent with these findings, CD146+iMSCs may modulate the IL-17 signaling pathway, thereby influencing downstream inflammatory networks.

Furthermore, PPI network analysis identified nine hub genes. Ex vivo experiments demonstrated that CD146+iMSCs significantly suppressed the expression of these genes in inflammatory intestinal epithelial cells. Most of these genes have been previously reported to be involved in processes such as inflammasome activation [57], pyroptosis [58], and immune cell recruitment [59]. For instance, GBP1 promotes pyroptosis in UC [58], and CXCL10 exacerbates intestinal inflammation by facilitating Th1 response and effector cell recruitment [60]. These findings suggest that suppressing these hub genes may represent a key molecular mechanism through which CD146+iMSCs alleviate intestinal inflammation, warranting further investigation into their potential therapeutic value.

In terms of immune regulation, macrophage polarization plays a critical role in the pathogenesis of UC [61]. Our immune infiltration analysis revealed significantly increased pro-inflammatory M1 macrophages in UC patients. CD146+iMSCs inhibit LPS-induced M1 polarization and promote IL-4-induced M2 polarization ex vivo. This mechanism may involve mediators secreted by iMSCs, such as tumor necrosis factor-inducible gene 6 protein (TSG-6) and PGE2, which have been reported to promote the transition of macrophages toward an anti-inflammatory phenotype [62–64]. Notably, this study also revealed that CD146+iMSCs inhibit the cGAS–STING signaling pathway, which is involved in innate immunity [65] and has been recently implicated in M1 macrophage polarization [66–68]. Western blot results showed that the protein expression of cGAS and STING was significantly downregulated in an inflammatory intestinal epithelial cell model following treatment with CD146+iMSCs, suggesting that these cells may regulate macrophage polarization and ultimately attenuate colonic inflammation by suppressing this pathway.

In summary, CD146+iMSCs may exert their therapeutic effects through multiple coordinated mechanisms, including suppression of the IL-17 signaling pathway, downregulation of multiple inflammation-related hub genes, and modulation of macrophage polarization via the cGAS–STING pathway. However, the inter-regulatory relationships among these pathways and their in vivo significance require further high-quality basic research to elucidate the underlying mechanisms.

Findings of this study provide preclinical evidence supporting the therapeutic potential of CD146+iMSCs in ulcerative colitis; however, several limitations remain. First, although transcriptomic analysis and ex vivo experiments suggested potential mechanisms involving the IL-17 signaling pathway, hub genes, and macrophage polarization, the direct target cell types of CD146+iMSCs and their upstream and downstream regulatory pathways remain unclear. Furthermore, functional validation through in vivo gene knock-out is lacking, and the specific contributions of these pathways in the disease context require further elucidation. Second, while ex vivo biological characteristics were compared between CD146+iMSCs and CD146+UCMSCs, a direct in vivo

comparison of therapeutic efficacy was lacking, making it difficult to evaluate their translational potential comprehensively. Finally, the iMSCs used in this study were likely derived from a single donor's commercial iPSCs line. While this ensures consistent cell quality and minimal heterogeneity, caution is warranted when generalizing these conclusions to iMSCs derived from other iPSC sources. Additionally, the mismatch in the number of donors between the two cell groups may affect the generalizability of the RNA-sequencing data.

Given the aforementioned limitations, future research can be advanced in multiple directions in greater depth. First, the specific mechanisms by which CD146+iMSCs regulate the IL-17 signaling pathway and macrophage polarization in vivo should be further elucidated. Secondly, the donor sources of iPSCs should be expanded to establish a multi-donor CD146+iMSCs bank. A systematic comparison should then be conducted between these CD146+iMSCs and CD146+MSCs derived from various tissues—such as umbilical cord, bone marrow, and adipose tissue—in terms of their biological characteristics and efficacy in treating ulcerative colitis. Furthermore, transcriptomic analyses of multi-donor CD146+iMSCs and tissue-derived CD146+MSCs should be conducted. These efforts may be integrated with high-dimensional technologies such as proteomics and single-cell RNA sequencing to deeply investigate the unique molecular expression profiles of CD146+iMSCs and their therapeutic mechanisms. This will ultimately facilitate the development and clinical application of CD146+iMSCs-based therapeutic regimens for inflammatory diseases.

Conclusion

This study demonstrated that CD146+iMSCs possess superior proliferative capacity and differentiation potential compared to CD146+UCMSCs, while effectively ameliorating DSS-induced UC in mice by restoring intestinal barrier function and suppressing inflammation. These therapeutic effects may be mediated through modulation of the IL-17 signaling pathway, inhibiting key inflammatory hub genes, and regulating macrophage polarization via the cGAS-STING pathway. These findings highlight the promise of CD146+iMSCs as a cell-based therapeutic strategy for inflammatory bowel diseases, warranting further investigation into their clinical translational potential.

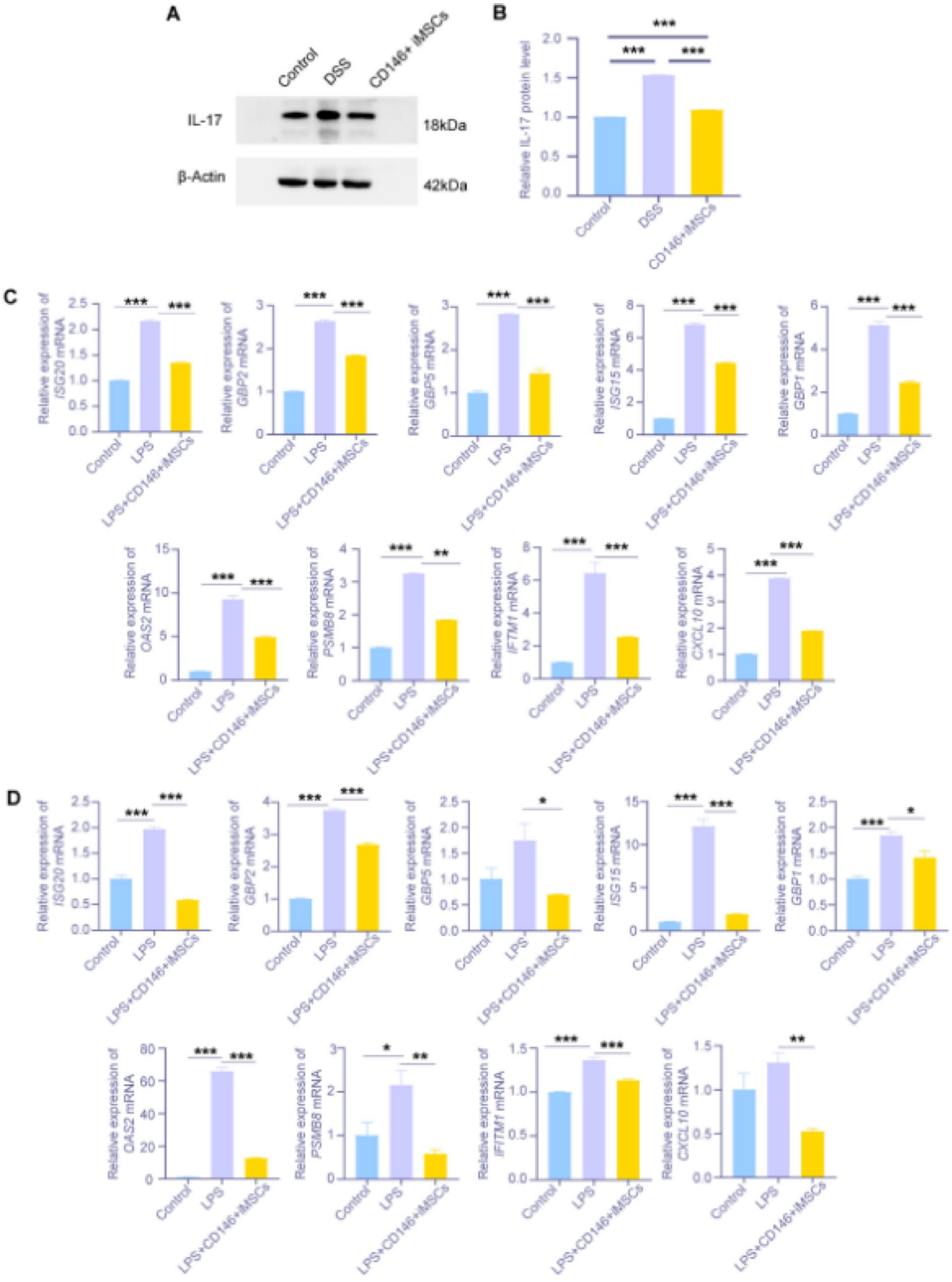

Fig. 7 Transcriptome analysis of ulcerative colitis. **A** Expression of IL-17 protein in the colon tissues of UC group, control group, and CD146+iMSCs group. **B** Quantitative analysis of the expression level of IL-17 protein. **C** HUB genes mRNA expression in HIEC cells post DSS induction and CD146+iMSCs treatment, as measured by RT-PCR ($n=4$ in each group). **D** HUB genes mRNA expression in IEC-6 cells post DSS induction and CD146+iMSCs treatment, as measured by RT-PCR ($n=4$ in each group). *$p<0.05$, **$p<0.01$, ***$p<0.001$

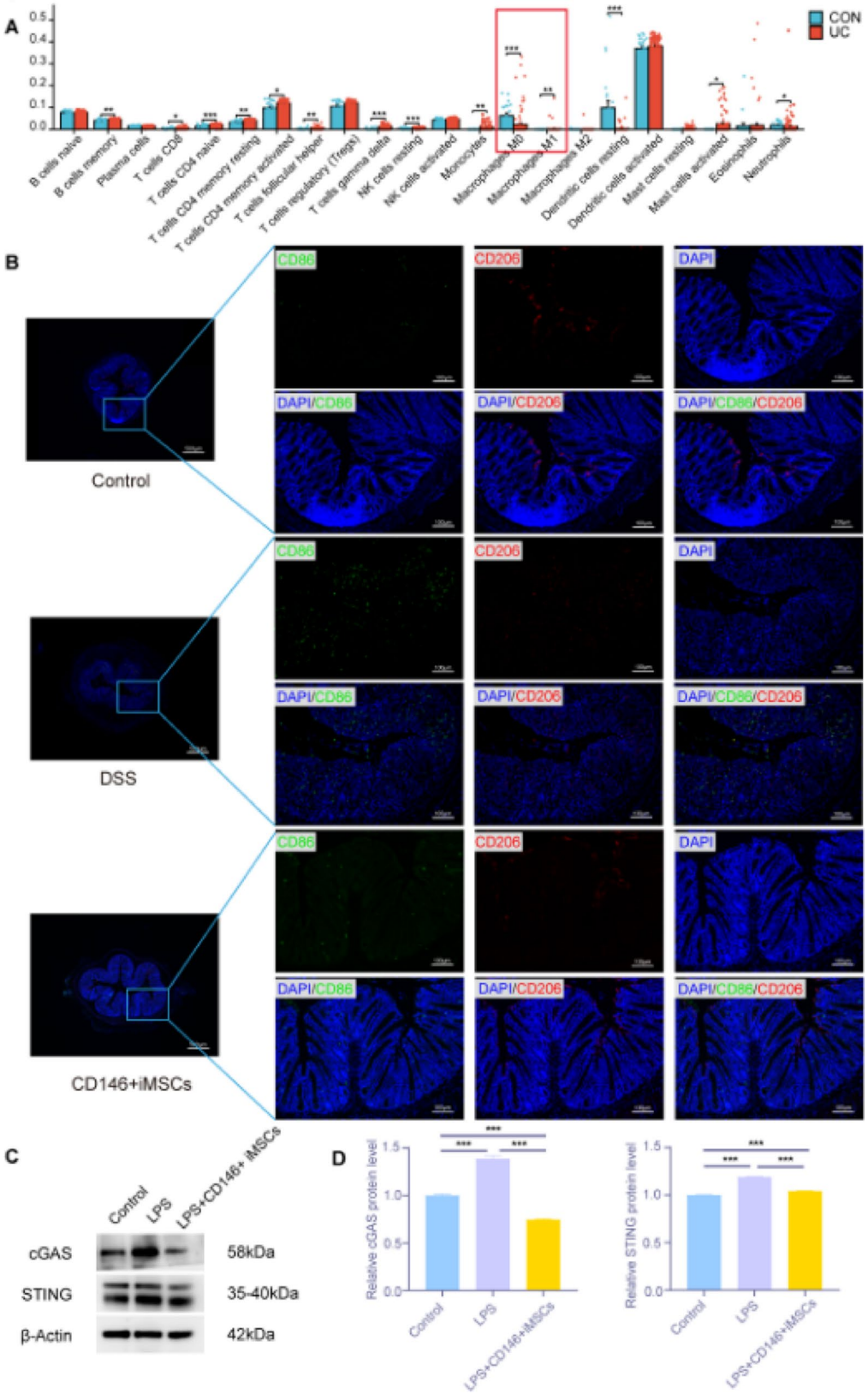

Fig. 8 CD146+iMSCs regulate macrophage polarization through cGAS-STING axis. **A** Immune infiltration analysis of four UC datasets. **B** Immunofluorescence images of macrophage infiltration in colonic tissues. **C** Western Blot analysis of expression level of cGAS and STING protein. **D** Quantitative statistics were performed for gray values of cGAS and STING protein. *$p < 0.05$, **$p < 0.01$, ***$p < 0.001$

Abbreviations

UC	Ulcerative colitis
IBD	Inflammatory bowel disease
MSCs	Mesenchymal stem cells
iPSCs	Induced pluripotent stem cells
iMSCs	Induced pluripotent stem cells-derived mesenchymal stem cells
BMSCs	Bone marrow mesenchymal stem cells
PGE2	Prostaglandin E2
UCMSCs	Umbilical cord mesenchymal stem cells
MACS	Magnetic activated cell sorting
LPS	Lipopolysaccharide
IL	Interleukin
RT-PCR	Real-time quantitative polymerase chain reaction
FPKM	Fragments per kilobase of exon per million mapped fragments
FC	Fold change
DSS	Dextran sodium sulfate
DAI	Disease activity index
H&E	Hematoxylin and eosin
ELISA	Enzyme-linked immunosorbent assay
TNF-α	Tumor necrosis factor-alpha
DEGs	Differentially expressed genes
PCA	Principal component analysis
PPI	Protein-protein interaction
STRING	Search tool for the retrieval of interacting genes
GO	Gene ontology
KEGG	Kyoto Encyclopedia of Genes and Genomes
WB	Western Blot
HRP	Horseradish peroxidase
ECL	Enhanced chemiluminescence
M ± SEM	Mean ± standard error
ISCT	International Society for Cellular Therapy
CC	Cellular components
MF	Molecular functions
ZO-1	Zonula Occludens-1
WBC	White blood cell
RBC	Red blood cell
PLT	Platelet
HGB	Hemoglobin
TSG-6	Tumor necrosis factor alpha-stimulated gene-6

Supplementary Information

The online version contains supplementary material available at https://doi.org/10.1186/s13287-025-04695-7.

Supplementary Material 1.

Supplementary Material 2.

Supplementary Material 3.

Supplementary Material 4.

Acknowledgements

The authors declare that they have not used AI-generated work in this manuscript.

Author contributions

FJX, LZ and LS designed the research; LT and YMW performed the experiment and collected the data; LT, YXL and XCC performed the statistical analysis; LT and MRZ wrote the manuscript. LD and JF assisted with the literature searches and revised the manuscript. All authors read and approved the final manuscript.

Funding

This study was supported by the Healthcare Project Fund of the Department of Logistics Support (21BJZ50).

Data availability

The datasets (GSE9452, GSE87466, GSE36807 and GSE47908) analyzed during the current study are available in the GEO (https://www.ncbi.nlm.nih.gov/geo/). The authors confirm that the new RNA sequencing data supporting the findings of this study are available within the article and its supplementary materials (Supplementary file 2 and 3). Full-length blots/gels are presented in Supplementary file 4.

Declarations

Ethics approval and consent to participate

Clinical Ethics declaration: (1) Title of the approved project: Postpartum Umbilical Cord Collection. (2) Name of the institutional approval committee or unit: Medical Ethics Committee of Beijing Shangdi Hospital. (3) Approval number: SDEC-KT- 2023-2-S02. (4) Date of approval: 2023.05.16. This research has obtained relevant ethics approval, and the patient or his/her guardian/legally authorized representative/next of kin has provided written informed consent for participating in the research and/or using samples. For human iMSCs, Nuwacell Ltd. has confirmed that there was initial ethical approval for collection of human cells, and that the donors had signed informed consent. Animal Ethics declaration: (1) Title of the approved project: Biological characteristics of iPSC-derived CD146+ mesenchymal stem cells and efficacy and mechanism of treatment of ulcerative colitis. (2) Name of the institutional approval committee or unit: Ethics Committee of the Laboratory Animal Centre of the Academy of Military Medical Sciences. (3) Approval number: IACUC-DWZX-2023-571. (4) Date of approval: November 29, 2023. The protocols for animal experiments adhere to the ARRIVE (Animal Research: Reporting of in Vivo Experiments) guidelines.

Consent for publication

Not applicable.

Competing interests

The authors declare no competing interests.

Author details

[1]Institute of Fundamental and Frontier Sciences, University of Electronic Science and Technology of China, Chengdu 611731, People's Republic of China
[2]School of Nursing, Jilin University, Changchun 130021, People's Republic of China
[3]Department of Experimental Hematology and Biochemistry, Beijing Institute of Radiation Medicine, Beijing 100850, People's Republic of China
[4]Department of Gastroenterology, The First Medical Center of PLA General Hospital, Beijing 100853, People's Republic of China
[5]Department of Respiratory and Critical Care, Quzhou Affiliated Hospital of Wenzhou Medical University, Quzhou 324000, People's Republic of China

Received: 19 June 2025 / Accepted: 22 September 2025
Published online: 14 October 2025

References

1. Ordás I, Eckmann L, Talamini M, Baumgart DC, Sandborn WJ. Ulcerative colitis. Lancet. 2012;380(9853):1606–19.
2. Popov J, Caputi V, Nandeesha N, Rodriguez DA, Pai N. Microbiota-immune interactions in ulcerative colitis and colitis associated cancer and emerging microbiota-based therapies. Int J Mol Sci. 2021;22(21):11365.
3. Jairath V, Feagan BG. Global burden of inflammatory bowel disease. Lancet Gastroenterol Hepatol. 2020;5(1):2–3.
4. Du L, Ha C. Epidemiology and pathogenesis of ulcerative colitis. Gastroenterol Clin North Am. 2020;49(4):643–54.
5. Kobayashi T, Siegmund B, Le Berre C, Wei SC, Ferrante M, Shen B, et al. Ulcerative colitis. Nat Rev Dis Primers. 2020;6(1):74.
6. Kaplan GG. The global burden of IBD: from 2015 to 2025. Nat Reviews Gastroenterol Hepatol. 2015;12(12):720–7.
7. Ng SC, Shi HY, Hamidi N, Underwood FE, Tang W, Benchimol EI, et al. Worldwide incidence and prevalence of inflammatory bowel disease in the 21st century: a systematic review of population-based studies. Lancet. 2017;390(10114):2769–78.
8. Chang JT. Pathophysiology of inflammatory bowel diseases. N Engl J Med. 2020;383(27):2652–64.

9. Dominici M, Le Blanc K, Mueller I, Slaper-Cortenbach I, Marini F, Krause D, et al. Minimal criteria for defining multipotent mesenchymal stromal cells. The international society for cellular therapy position statement. Cytotherapy. 2006;8(4):315–7.
10. Pittenger MF, Mackay AM, Beck SC, Jaiswal RK, Douglas R, Mosca JD, et al. Multilineage potential of adult human mesenchymal stem cells. Science. 1999;284(5411):143–7.
11. Biehl JK, Russell B. Introduction to stem cell therapy. J Cardiovasc Nurs. 2009;24(2):98–103. (quiz 4–5).
12. Zhang HM, Yuan S, Meng H, Hou XT, Li J, Xue JC, et al. Stem cell-based therapies for inflammatory bowel disease. Int J Mol Sci. 2022;23(15):8494.
13. Ko JZ, Johnson S, Dave M. Efficacy and safety of mesenchymal stem/stromal cell therapy for inflammatory bowel diseases: an up-to-date systematic review. Biomolecules. 2021;11(1):82.
14. Hidalgo-García L, Ruiz-Malagon AJ, Huertas F, Rodríguez-Sojo MJ, Molina-Tijeras JA, Diez-Echave P, et al. Administration of intestinal mesenchymal stromal cells reduces colitis-associated cancer in C57BL/6J mice modulating the immune response and gut dysbiosis. Pharmacol Res. 2023;195:106891.
15. Costa LA, Eiro N, Fraile M, Gonzalez LO, Saá J, Garcia-Portabella P, et al. Functional heterogeneity of mesenchymal stem cells from natural niches to culture conditions: implications for further clinical uses. Cell Mol Life Sci. 2021;78(2):447–67.
16. Sabapathy V, Kumar S. hiPSC-derived iMSCs: nextgen MSCs as an advanced therapeutically active cell resource for regenerative medicine. J Cell Mol Med. 2016;20(8):1571–88.
17. Kang R, Zhou Y, Tan S, Zhou G, Aagaard L, Xie L, et al. Mesenchymal stem cells derived from human induced pluripotent stem cells retain adequate osteogenicity and chondrogenicity but less adipogenicity. Stem Cell Res Ther. 2015;6(1):144.
18. Zhao C, Ikeya M. Generation and applications of induced pluripotent stem cell-derived mesenchymal stem cells. Stem Cells Int. 2018;2018:9601623.
19. Soontararak S, Chow L, Johnson V, Coy J, Wheat W, Regan D, et al. Mesenchymal stem cells (MSC) derived from induced pluripotent stem cells (iPSC) equivalent to adipose-derived MSC in promoting intestinal healing and Microbiome normalization in mouse inflammatory bowel disease model. Stem Cells Transl Med. 2018;7(6):456–67.
20. Zhu Y, Wang Y, Zhao B, Niu X, Hu B, Li Q, et al. Comparison of exosomes secreted by induced pluripotent stem cell-derived mesenchymal stem cells and synovial membrane-derived mesenchymal stem cells for the treatment of osteoarthritis. Stem Cell Res Ther. 2017;8(1):64.
21. Frobel J, Hemeda H, Lenz M, Abagnale G, Joussen S, Denecke B, et al. Epigenetic rejuvenation of mesenchymal stromal cells derived from induced pluripotent stem cells. Stem Cell Rep. 2014;3(3):414–22.
22. Giuliani M, Oudrhiri N, Noman ZM, Vernochet A, Chouaib S, Azzarone B, et al. Human mesenchymal stem cells derived from induced pluripotent stem cells down-regulate NK-cell cytolytic machinery. Blood. 2011;118(12):3254–62.
23. Ng J, Hynes K, White G, Sivanathan KN, Vandyke K, Bartold PM, et al. Immunomodulatory properties of induced pluripotent stem cell-derived mesenchymal cells. J Cell Biochem. 2016;117(12):2844–53.
24. Chang YH, Wu KC, Ding DC. Induced pluripotent stem cell-differentiated chondrocytes repair cartilage defect in a rabbit osteoarthritis model. Stem Cells Int. 2020;2020:8867349.
25. Saetersmoen ML, Hammer Q, Valamehr B, Kaufman DS, Malmberg KJ. Off-the-shelf cell therapy with induced pluripotent stem cell-derived natural killer cells. Semin Immunopathol. 2019;41(1):59–68.
26. Espagnolle N, Guilloton F, Deschaseaux F, Gadelorge M, Sensébé L, Bourin P. CD146 expression on mesenchymal stem cells is associated with their vascular smooth muscle commitment. J Cell Mol Med. 2014;18(1):104–14.
27. Harkness L, Zaher W, Ditzel N, Isa A, Kassem M. CD146/MCAM defines functionality of human bone marrow stromal stem cell populations. Stem Cell Res Ther. 2016;7:4.
28. Wangler S, Menzel U, Li Z, Ma J, Hoppe S, Benneker LM, et al. CD146/MCAM distinguishes stem cell subpopulations with distinct migration and regenerative potential in degenerative intervertebral discs. Osteoarthritis Cartilage. 2019;27(7):1094–105.
29. Lehmann JM, Riethmüller G, Johnson JP. MUC18, a marker of tumor progression in human melanoma, shows sequence similarity to the neural cell adhesion molecules of the Immunoglobulin superfamily. Proc Natl Acad Sci U S A. 1989;86(24):9891–5.
30. Nollet M, Stalin J, Moyon A, Traboulsi W, Essaadi A, Robert S, et al. A novel anti-CD146 antibody specifically targets cancer cells by internalizing the molecule. Oncotarget. 2017;8(68):112283–96.
31. Zeng P, Li H, Lu PH, Zhou LN, Tang M, Liu CY, et al. Prognostic value of CD146 in solid tumor: a systematic review and meta-analysis. Sci Rep. 2017;7(1):4223.
32. Stalin J, Traboulsi W, Vivancos-Stalin L, Nollet M, Joshkon A, Bachelier R, et al. Therapeutic targeting of soluble CD146/MCAM with the M2J-1 monoclonal antibody prevents metastasis development and procoagulant activity in CD146-positive invasive tumors. Int J Cancer. 2020;147(6):1666–79.
33. Elshal MF, Khan SS, Takahashi Y, Solomon MA, McCoy JP Jr. CD146 (Mel-CAM), an adhesion marker of endothelial cells, is a novel marker of lymphocyte subset activation in normal peripheral blood. Blood. 2005;106(8):2923–4.
34. Gabsi A, Heim X, Dlala A, Gati A, Sakhri H, Abidi A, et al. TH17 cells expressing CD146 are significantly increased in patients with systemic sclerosis. Sci Rep. 2019;9(1):17721.
35. Covas DT, Panepucci RA, Fontes AM, Silva WA Jr., Orellana MD, Freitas MC, et al. Multipotent mesenchymal stromal cells obtained from diverse human tissues share functional properties and gene-expression profile with CD146+ perivascular cells and fibroblasts. Exp Hematol. 2008;36(5):642–54.
36. Tsang WP, Shu Y, Kwok PL, Zhang F, Lee KK, Tang MK, et al. CD146+ human umbilical cord perivascular cells maintain stemness under hypoxia and as a cell source for skeletal regeneration. PLoS ONE. 2013;8(10):e76153.
37. Wu CC, Liu FL, Sytwu HK, Tsai CY, Chang DM. CD146+ mesenchymal stem cells display greater therapeutic potential than CD146-cells for treating collagen-induced arthritis in mice. Stem Cell Res Ther. 2016;7:23.
38. Wu YX, Jing XZ, Sun Y, Ye YP, Guo JC, Huang JM, et al. CD146+ skeletal stem cells from growth plate exhibit specific chondrogenic differentiation capacity in vitro. Mol Med Rep. 2017;16(6):8019–28.
39. Du Y, Rong L, Cong Y, Shen L, Zhang N, Wang B. Macrophage polarization: an effective approach to targeted therapy of inflammatory bowel disease. Expert Opin Ther Targets. 2021;25(3):191–209.
40. Zhang L, Zhang X, Liu Y, Zhang W, Wu C-T, Wang L. CD146+ umbilical cord mesenchymal stem cells exhibit high Immunomodulatory activity and therapeutic efficacy in septic mice. J Inflamm Res. 2023;16:579–94.
41. Bowles AC, Kouroupis D, Willman MA, Perucca Orfei C, Agarwal A, Correa D. Signature quality attributes of CD146+ mesenchymal stem/stromal cells correlate with high therapeutic and secretory potency. Stem Cells. 2020;38(8):1034–49.
42. Zhang L, Sun Y, Zhang X-X, Liu Y-B, Sun H-Y, Wu C-T, et al. Comparison of CD146 +/- mesenchymal stem cells in improving premature ovarian failure. Stem Cell Res Ther. 2022;13(1):267.
43. Wirtz S, Popp V, Kindermann M, Gerlach K, Weigmann B, Fichtner-Feigl S, et al. Chemically induced mouse models of acute and chronic intestinal inflammation. Nat Protoc. 2017;12(7):1295–309.
44. Rajasingh S, Sigamani V, Selvam V, Gurusamy N, Kirankumar S, Vasanthan J, et al. Comparative analysis of human induced pluripotent stem cell-derived mesenchymal stem cells and umbilical cord mesenchymal stem cells. J Cell Mol Med. 2021;25(18):8904–19.
45. Wang P, Zhang Y, Li Z, Zhou S, Tang Q, Wang Z, et al. Mesenchymal stem cells derived from human urine-derived iPSCs exhibit low immunogenicity and reduced Immunomodulatory profile. Int J Mol Sci. 2024;25(19):10394.
46. Lian Q, Zhang Y, Zhang J, Zhang HK, Wu X, Zhang Y, et al. Functional mesenchymal stem cells derived from human induced pluripotent stem cells attenuate limb ischemia in mice. Circulation. 2010;121(9):1113–23.
47. Shao K, Koch C, Gupta MK, Lin Q, Lenz M, Laufs S, et al. Induced pluripotent mesenchymal stromal cell clones retain donor-derived differences in DNA methylation profiles. Mol Ther. 2013;21(1):240–50.
48. Gonzalez-Rey E, Anderson P, González MA, Rico L, Büscher D, Delgado M. Human adult stem cells derived from adipose tissue protect against experimental colitis and sepsis. Gut. 2009;58(7):929–39.
49. Misra DP, Agarwal V. Th17.1 lymphocytes: emerging players in the orchestra of immune-mediated inflammatory diseases. Clin Rheumatol. 2022;41(8):2297–308.
50. Johansen C, Usher PA, Kjellerup RB, Lundsgaard D, Iversen L, Kragballe K. Characterization of the interleukin-17 isoforms and receptors in lesional psoriatic skin. Br J Dermatol. 2009;160(2):319–24.
51. Liu C, Qian W, Qian Y, Giltiay NV, Lu Y, Swaidani S, et al. Act1, a U-box E3 ubiquitin ligase for IL-17 signaling. Sci Signal. 2009;2(92):ra63.
52. Amatya N, Garg AV, Gaffen SL. IL-17 signaling: the Yin and the Yang. Trends Immunol. 2017;38(5):310–22.
53. Huangfu L, Li R, Huang Y, Wang S. The IL-17 family in diseases: from bench to bedside. Signal Transduct Target Ther. 2023;8(1):402.
54. Qin Z, Wang PY, Wan JJ, Zhang Y, Wei J, Sun Y, et al. MicroRNA124-IL6R mediates the effect of nicotine in inflammatory bowel disease by shifting Th1/Th2 balance toward Th1. Front Immunol. 2020;11:235.

55. Terraza-Aguirre C, Campos-Mora M, Elizondo-Vega R, Contreras-López RA, Luz-Crawford P, Jorgensen C, et al. Mechanisms behind the immunoregulatory dialogue between mesenchymal stem cells and Th17 cells. Cells. 2020;9(7):1660.
56. Hua C, Liang Q, Chen S, Zhu J, Tang Y, Chen X, et al. Human umbilical cord mesenchymal stem cell treatment alleviates symptoms in an atopic dermatitis-like mouse model. Stem Cell Res Ther. 2023;14(1):147.
57. Li Y, Lin X, Wang W, Wang W, Cheng S, Huang Y, et al. The Proinflammatory role of guanylate-binding protein 5 in inflammatory bowel diseases. Front Microbiol. 2022;13:926915.
58. Ning Y, Lin K, Fang J, Chen X, Hu X, Liu L, et al. Pyroptosis-related signature predicts the progression of ulcerative colitis and colitis-associated colorectal cancer as well as the anti-TNF therapeutic response. J Immunol Res. 2023;2023:7040113.
59. Napolitano A, van der Veen AG, Bunyan M, Borg A, Frith D, Howell S, et al. Cysteine-reactive free ISG15 generates IL-1β-producing CD8α(+) DENDRITIC CELLS AT THE SITE OF infection. J Immunol. 2018;201(2):604–14.
60. Trivedi PJ, Adams DH. Chemokines and chemokine receptors as therapeutic targets in inflammatory bowel disease; pitfalls and promise. J Crohns Colitis. 2018;12(suppl2):S641–52.
61. Cao L, Xu H, Wang G, Liu M, Tian D, Yuan Z. Extracellular vesicles derived from bone marrow mesenchymal stem cells attenuate dextran sodium sulfate-induced ulcerative colitis by promoting M2 macrophage polarization. Int Immunopharmacol. 2019;72:264–74.
62. Song WJ, Li Q, Ryu MO, Nam A, An JH, Jung YC, et al. Canine adipose tissue-derived mesenchymal stem cells pre-treated with TNF-alpha enhance Immunomodulatory effects in inflammatory bowel disease in mice. Res Vet Sci. 2019;125:176–84.
63. Li Y, Ma K, Zhang L, Xu H, Zhang N. Human umbilical cord blood derived-mesenchymal stem cells alleviate dextran sulfate sodium-induced colitis by increasing regulatory T cells in mice. Front Cell Dev Biol. 2020;8:604021.
64. Cao X, Duan L, Hou H, Liu Y, Chen S, Zhang S, et al. IGF-1 C hydrogel improves the therapeutic effects of MSCs on colitis in mice through PGE(2)-mediated M2 macrophage polarization. Theranostics. 2020;10(17):7697–709.
65. Ou L, Zhang A, Cheng Y, Chen Y. The cGAS-STING pathway: a promising immunotherapy target. Front Immunol. 2021;12:795048.
66. Ohkuri T, Kosaka A, Nagato T, Kobayashi H. Effects of STING stimulation on macrophages: STING agonists polarize into classically or alternatively activated macrophages? Hum Vaccin Immunother. 2018;14(2):285–7.
67. Jing W, McAllister D, Vonderhaar EP, Palen K, Riese MJ, Gershan J, et al. STING agonist inflames the pancreatic cancer immune microenvironment and reduces tumor burden in mouse models. J Immunother Cancer. 2019;7(1):115.
68. Shen X, Sun C, Cheng Y, Ma D, Sun Y, Lin Y, et al. cGAS mediates inflammation by polarizing macrophages to M1 phenotype via the mTORC1 pathway. J Immunol. 2023;210(8):1098–107.

Publisher's note